Robust feedback stabilization of an unmanned motorcycle

Running title: Motorcycle robust control

Uri Nenner, Raphael Linker(*) and Per-Olof Gutman

Division of Environmental, Water and Agricultural Engineering

Faculty of Civil and Environmental Engineering

Technion-Israel Institute of Technology

Haifa 32000, Israel

emails: nenner@tx.technion.ac.il, linkerr@tx.technion.ac.il, peo@technion.ac.il

(*) corresponding author

Tel: +972 4 8295902

Fax: +972 4 8228898

Abstract

This paper details the design and implementation of a robust controller that stabilizes an unmanned motorcycle. A linearized model and Quantitative Feedback Theory (QFT) are used to derive a low order cascaded controller that stabilizes the motorcycle for velocities ranging from 2.5 to 6.5 [m/s]. Stabilization is achieved by measuring the roll angle and roll rate and controlling the steering torque. The approach is validated through simulations and experiments with a 50cc scooter whose throttle, brakes, and reference roll angle are radio-controlled.

Keywords: Quantitative Feedback Theory (QFT), cascade control, bicycle balancing, steering control, two-wheeled vehicle

1. Introduction

Two-wheeled vehicles, also called single track vehicles, are inherently unstable non-linear systems whose properties strongly depend on travel velocity, which makes the design of a stabilizing controller for such vehicles particularly challenging. Ruijs and Pacejka (1985) were probably the first to stabilize a motorcycle by feedback control. Getz and Marsden (1995) developed a controller that used both steering angle and forward speed to control a riderless bicycle, allowing it to track an arbitrary path without falling over. In order to achieve this, Getz and Marsden (1995) derived nonlinear equations of motion of a highly simplified model that considered the bicycle as a point mass with zero trail and rake angles and did not consider wheel radius and wheel inertia . Beznos et al. (1998) designed an autonomous, front wheel driven bicycle incorporating zero trail and steering axis angle, balanced in a vertical position by two mechanical gyroscopes serving as actuators that created a roll moment opposing the gravity-induced roll moment. Chidzonga and Eitelberg (2003) investigated the possibility of stabilizing a riderless bicycle at rest by controlling the velocity (small velocity perturbations around zero) when the front wheel is steered at a fixed angle. Their work was based on a point mass, zero-trail bicycle model. Miyagishi, Kageyama, Takama, Baba and Uchiyama (2003) used a proportional-derivative controller to control the roll angle of an unmanned motorcycle traveling at speeds up to 8 m/s. A particularity of their work was that they did not apply the steering torque directly to the steering shaft but rather included a spring-damper system emulating the rider's arm. Tanaka and Murakami (2004) presented a basic point-mass bicycle model in which the bicycle was considered as a point-mass

pendulum, and its roll dynamic equation was based on the gravitational and centripetal forces. The latter was associated with the radius of curvature of the bicycle's path, which in turn was associated with the steering angle by a geometric constraint. A proportional-derivative controller with a disturbance observer was designed to balance the bicycle in an upright position in an indoor laboratory setup. Iuchi et al. (2005) presented a multiple input-multiple output (MIMO) two degree of freedom (2DOF) control scheme, using both steering angle and center-of-gravity lateral shifting in order to keep a bicycle upright. The bicycle was modeled as double point-mass inverted pendulums, attached to a front wheel that included wheel inertia, mass and trail, although not all the moments existing in a steered bicycle due to trail were considered in the model. The angular accelerations of both the steering and the upper pendulum angles were used as control variables to keep the bicycle upright, and successful experiments were reported in their paper. Yi, Song, Levandowski and Jayasuriya (2006) presented a trajectory tracking and balancing control algorithm for an autonomous motorcycle. Yi et al. (2006) used an extension of the bicycle model derived in Getz and Marsden (1995) in which rake angle and trail were included. A controller based on the steering angle and the rear wheel torque was derived in order to track an arbitrary trajectory while maintaining stability. This control system was validated by numerical simulations and was implemented on a motorcycle that entered a DARPA autonomous vehicle competition (see http://www.ghostriderrobot.com).

Contrary to the above studies that were based on very simplified models, recent works have also considered the use of highly complex multi-body dynamics models such as the one developed by Sharp and Limebeer (2001). Sharp, Evangelou and Limebeer

(2004) used such a model to design and validate a feedback proportional-integral-derivative (PID) controller for controlling the steering torque based on roll angle measurement. The parameters of the controller were speed-dependant in order to achieve stability over a wide range of speeds. Sharp (2006, 2007, 2007b) used a similar model to develop optimal control strategies for either path tacking or speed tracking using road preview.

This paper presents the design and validation of a cascaded single input-single output (SISO) control scheme that stabilizes a motorcycle over a predefined range of forward velocities. The controlled and control variables are the roll angle and the steering torque, respectively. Although the MIMO approach followed by Iuchi et al. (2005), i.e. steering angle and lateral shift of center of gravity, may seem closer to human operation, it must be noted that in that configuration the response times of the two loops greatly differ. Indeed, Weir (1972) and Sharp (2001, 2006, 2007) showed that motorcycle steering is achieved mainly through the steering torque, while body-induced shift of the center of gravity is secondary. This can be intuitively demonstrated by considering two situations in which the rider would guide a motorcycle either only by shifting his body without touching the handle bars, or only by applying a steering torque while keeping his body rigid relative to the frame. Clearly, much better tracking results would be achieved in the second case.

The controller design in this paper is based on a linearized model in which the rake angle and trail are not neglected, and mass distribution and wheels inertia are taken into account. All the model parameters depend on the forward velocity and are therefore time-varying. In addition, almost all the parameters depend on motorcycle

properties that are difficult to estimate accurately, such as moments of inertia and products of inertia. Therefore, the two viable control approaches are either adaptive control, which should preferably include measurement of the forward velocity, or robust control. In the present study, the latter approach was selected, mostly because it is difficult to design an adaptive controller that does not make the closed loop exhibit tendencies to instability during the adaptation phase (Gutman, 2003), particularly when the controlled system is inherently unstable as in the present case. Of the various methods for designing robust controllers, the Quantitative Feedback Theory (QFT) approach (Horowitz, 1993; Horowitz and Sidi, 1972) was chosen since it offers a highly transparent design process that enables the designer to reach good results with simple, low order compensators.

2. Experimental prototype

The experimental prototype consisted of a 50cc scooter with automatic variable transmission that was retrofitted to be operated by remote and automatic control. A microchip PIC18F8520 microprocessor was installed on the motorcycle, and received roll angle reference, throttle, and brake commands via an R/C receiver. The throttle and brake loops were controlled manually by the user via the R/C, while the roll angle was automatically controlled to follow the roll angle reference given over the R/C. The roll angle was measured by a dynamic gyro-enhanced inclinometer (Microstrain FAS-G) and the roll rate was measured using a vibrating ring gyroscope (Silicon Sensing Systems, CRS02). Both analog signals were acquired by the microcontroller at a sampling frequency of 10 kHz, and averaged over disjoint 20 ms periods, yielding an effective sampling frequency of 50Hz. Every 20ms, the microcontroller, which was

programmed in the C language, issued pulse width modulated (PWM) commands to the throttle, brake and steering motors via appropriate H-bridges. Steering was controlled by a 24V DC motor with a 1:45 reduction transmission gear (Figure 1).

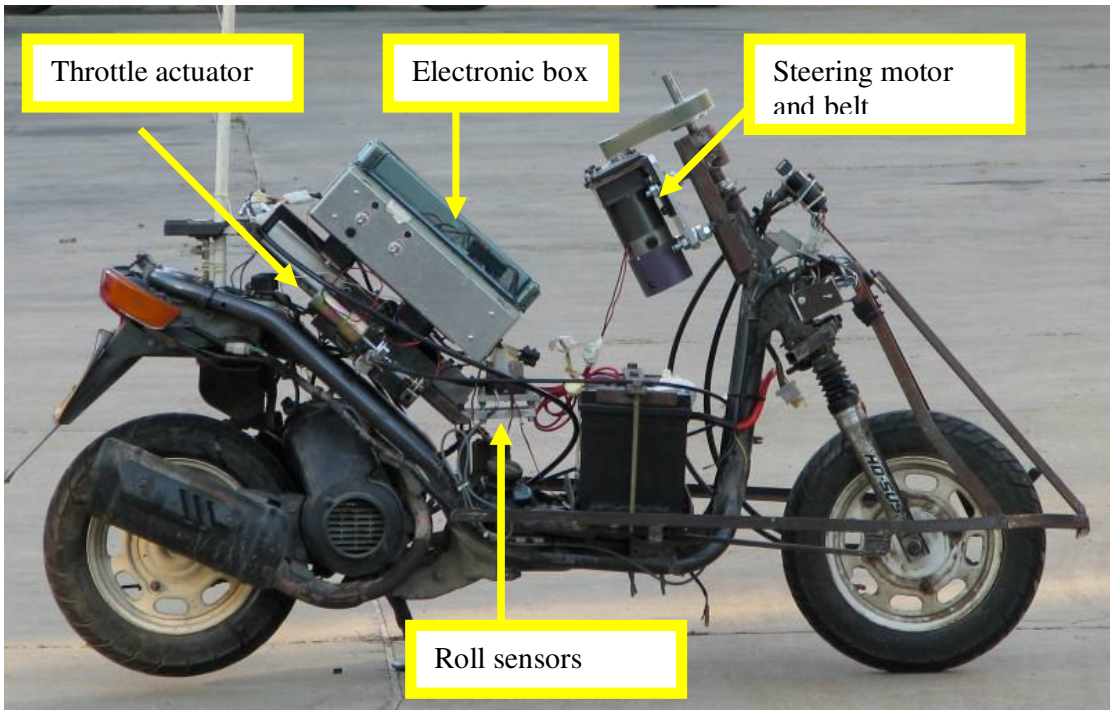

Figure 1: Side view of the experimental prototype

The properties of the motorcycle prototype (Table 1) were estimated either through direct measurements, e.g. physical dimensions and centers of mass; or by Computer Aided Design (CAD) models based on the measurements, e.g. calculation of the moments of inertia.

Table 1: Motorcycle parameters (see Figure 2 for a geometric description of the mechanical parameters)

Parameter	Description	Value	Uncertainty range

Parameters of the steering DC motor

J_m	Armature inertia	102.3 $\left[Kg \cdot mm^2\right]$	None
k_b	Back EMF constant	0.0847 $\left[\frac{V}{rad/\mathrm{s}}\right]$	None
k_t	Torque constant	0.0847 $\left[\frac{Nm}{A}\right]$	None
L	Armature inductance	2.18 $[mH]$	None
N	Transmission reduction (Motor gearhead and timing pullies pulleys combined)	45	None
R	Armature Resistance	4.887 $[\Omega]$	None

Other parameters of the motorcycle

c_f	Mechanical trail	86.53 $[mm]$	None
c_w	Wheel base	1.08 $[m]$	None
d	Perpendicular distance from the steering axis to the front assembly's center of mass	4.5 $[mm]$	None
h_f	Height of the front assembly center of mass relative to the front wheel contact point	0.4110 $[m]$	None

h_r	Height of the rear assembly center of mass relative to the rear wheel contact point	0.4096 $[m]$	±15%
I_{xx_2}	Rear wheel moment of inertia, measured about wheel axle	0.0431 $[kg \cdot m^2]$	None
I_{yy_f}	y'-y' moment of inertia of the front assembly, measured about front center of mass	1.1467 $[kg \cdot m^2]$	±15%
I_{yz_f}	y'-z' product of inertia of front assembly, measured about front center of mass.	-0.012 $[kg \cdot m^2]$	None
I_{zz_f}	z'-z' moment of inertia of the front assembly, measured about front assembly center of mass	0.0530 $[kg \cdot m^2]$	±15%
I_{yy_r}	y-y moment of inertia of the rear assembly, measured about rear center of mass	4.7235 $[kg \cdot m^2]$	±15%
I_{yz_r}	y-z product of inertia of rear assembly, measured about rear center of mass.	0.2204 $[kg \cdot m^2]$	None
I_{zz_r}	z-z moment of inertia of the rear assembly, measured about rear assembly center of mass	11.2341 $[kg \cdot m^2]$	±15%
l_f	Forward distance of the front assembly center of mass relative to the front	-0.1073 $[m]$	None

	wheel contact point		
l_r	Forward distance of the rear assembly center of mass relative to the rear wheel contact point	$0.4\ [m]$	±15%
m_f	Mass of front assembly	$13.9242\ [kg]$	±5%
m_r	Mass of rear assembly	$105.3572\ [kg]$	±15%
r_f	Front wheel radius	$0.205\ [m]$	None
r_r	Rear wheel radius	$0.205\ [m]$	None
λ	Steering head angle (also called Rake angle)	27°	None

At the controller design stage, parameters with very low uncertainty were considered without uncertainty, while uncertainty was considered in others (Table 1). It was assumed (1) that the front assembly parameters were known to a better extent since the protective shield attached to the rear assembly was modified several times, (2) that small uncertainties in the y-z products of inertia, of both the rear and front assemblies, have a small effect on the plant uncertainty, and (3) that a small uncertainty in the rear wheel inertia contributes very little to the overall plant uncertainty, as it is the front wheel that is being steered. These assumptions were verified by keeping all other parameters constant and plotting plant cases with 15% uncertainty in the above parameters. Very little plant uncertainty was observed, which confirmed the

assumption that uncertainty in these parameters contributed very little to the overall plant uncertainty.

3. The model

In order to design and test the control loop, a dynamic model of the motorcycle was derived under the following assumptions:

1. The motorcycle consists of four rigid bodies that are interconnected by friction-free hinge joints: The rear frame and motor; the front fork and steering shaft; the rear wheel; and the front wheel.
2. For the analysis, these four bodies are grouped into two bodies which are interconnected via the steering axis. These are the rear assembly, which consists of the rear frame, the motor and the rear wheel, and the front assembly, which consists of the front fork, the steering axis and the front wheel.
3. The dynamic properties of the rear and front suspensions are neglected. Suspensions are assumed to be fixed at their nominal deflection for the motorcycle self weight.
4. The wheels are considered as rigid discs, with knife-edge outer edges.
5. Both wheels remain in contact with the road at all times.
6. The road is rigid, flat and horizontal.
7. The forward velocity is constant or changing slowly.
8. There exists enough friction between the wheels and road to prevent sliding.
9. Only small perturbations from vertical straight ahead motion are considered.
10. When no steering is applied, the motorcycle is symmetric about a plane passing lengthwise through the middle of the rear frame.

Note that the differences between assuming pure-rolling wheels and side-slipping wheels are exposed in Sharp (1971). Under these assumptions, using the symbols defined in Table 1 and Figure 2, the following linearized roll and steering equations are obtained (Meijaard, Papadopoulos, Ruina and Schwab 2007; Nenner, 2009; Nenner, Linker and Gutman, 2009)

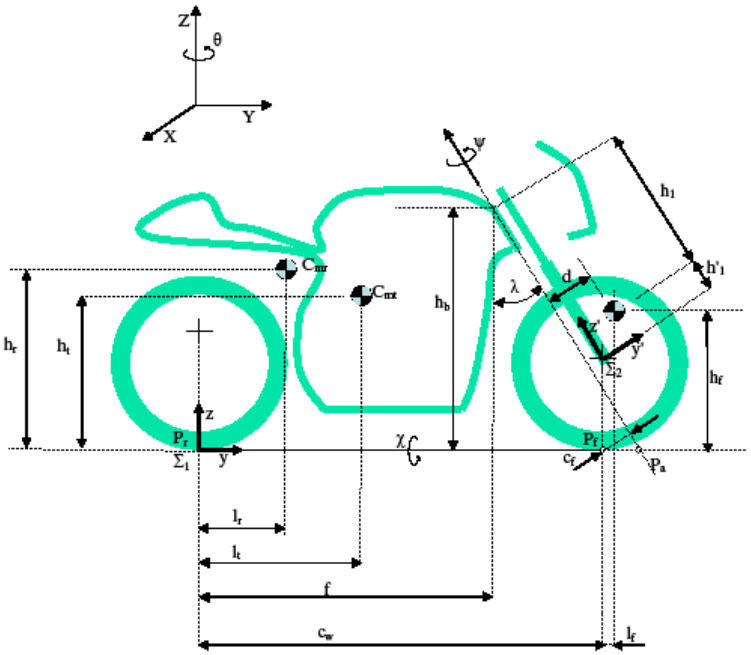

Figure 2: Motorcycle physical parameters.

Roll equation:

$$T_{yy}\ddot{\chi} - m_t g h_t \chi + \left(F'_{\lambda y} + T_{yz}\frac{C_f}{C_w}\right)\dot{\psi} + V\left(T_{yz}\frac{\cos\lambda}{C_w} - \frac{C_f}{C_w}\left(\frac{I_{xx_1}}{r_f} + \frac{I_{xx_2}}{r_r} + n\frac{I_{xx_3}}{r_r}\right) - \frac{I_{xx_1}}{r_f}\cos\lambda - m_t h_t \frac{C_f}{C_w}\right)\dot{\psi} +$$

$$+V^2\left(-\frac{Cos\lambda}{C_w}\left(\frac{I_{xx_1}}{r_f} + \frac{I_{xx_2}}{r_r} + n\frac{I_{xx_3}}{r_r}\right) - m_t h_t \frac{\cos\lambda}{C_w}\right)\psi + gv\psi = M_\chi \qquad (1)$$

Steering equation:

$$\left(F'_{\lambda\lambda}+2F''_{\lambda z}\frac{C_f}{C_w}+T_{zz}\frac{C_f^{\,2}}{C_w^{\,2}}\right)\ddot{\psi}+V\left(F''_{\lambda z}\frac{\cos\lambda}{C_w}+m_f d\frac{C_f}{C_w}+T_{zz}\frac{C_f}{C_w^{\,2}}\cos\lambda+m_t l_t\frac{C_f^{\,2}}{C_w^{\,2}}\right)\dot{\psi}+\mathrm{K}$$
$$\mathrm{K}+V^2\left(\frac{I_{xx1}}{r_f}\frac{\cos\lambda}{C_w}\sin\lambda+m_f d\frac{\cos\lambda}{C_w}+m_t l_t\frac{C_f}{C_w^{\,2}}\cos\lambda\right)\psi-\left(g\nu\sin\lambda\right)\psi+\left(F'_{\lambda y}+T_{yz}\frac{C_f}{C_w}\right)\ddot{\chi}+\mathrm{K}$$
$$\mathrm{K}+V\left(\frac{I_{xx_1}}{r_f}\cos\lambda+(\frac{I_{xx_1}}{r_f}+\frac{I_{xx_2}}{r_r}+n\frac{I_{xx_3}}{r_r})\frac{C_f}{C_w}\right)\dot{\chi}+g\nu\chi=M_\psi \tag{2}$$

Collecting terms, Equations (1) and (2) are rewritten as

$$M_{\chi\chi}\ddot{\chi}+M_{\chi\psi}\ddot{\psi}+C_{\chi\chi}\dot{\chi}+C_{\chi\psi}\dot{\psi}+K_{\chi\chi}\chi+K_{\chi\psi}\psi=M_\chi \tag{3}$$

$$M_{\psi\chi}\ddot{\chi}+M_{\psi\psi}\ddot{\psi}+C_{\psi\chi}\dot{\chi}+C_{\psi\psi}\dot{\psi}+K_{\psi\chi}\chi+K_{\psi\psi}\psi=M_\psi \tag{4}$$

where

M_ψ is the steering torque about the steering axis, applied to the front assembly by the steering motor, (control input) and M_χ is an external roll disturbance moment. All the $M_{\bullet\bullet}$, $C_{\bullet\bullet}$ and $K_{\bullet\bullet}$ parameters depend on the physical properties of the motorcycle and on the forward velocity.

Some manipulations of (3) and (4) yield

$$\psi(s)=\frac{p_1(s)}{p_5(s)}M_\psi(s)-\frac{p_4(s)}{p_5(s)}M_\chi(s) \tag{5}$$

$$\dot{\psi}(s)=\frac{s\cdot p_1(s)}{p_5(s)}M_\psi(s)-\frac{s\cdot p_4(s)}{p_5(s)}M_\chi(s) \tag{6}$$

$$\dot{\chi}(s)=-\frac{p_2(s)}{p_1(s)}\dot{\psi}(s)+\frac{s}{p_1(s)}M_\chi(s) \tag{7}$$

where the following notations were introduced for clarity:

$$p_1(s) = M_{\chi\chi}s^2 + C_{\chi\chi}s + K_{\chi\chi} \tag{8}$$

$$p_2(s) = M_{\chi\psi}s^2 + C_{\chi\psi}s + K_{\chi\psi} \tag{9}$$

$$p_3(s) = M_{\psi\psi}s^2 + C_{\psi\psi}s + K_{\psi\psi} \tag{10}$$

$$p_4(s) = M_{\psi\chi}s^2 + C_{\psi\chi}s + K_{\psi\chi} \tag{11}$$

$$p_5(s) = p_1(s)\cdot p_3(s) - p_2(s)\cdot p_4(s) \tag{12}$$

Since the actuator that delivers M_ψ is a DC motor, the electrical and dynamical equations of a brushed DC motor are introduced:

$$T(t) = k_t \cdot i(t) \tag{13}$$

$$e_m(t) = k_b \cdot \omega_m(t) \tag{14}$$

$$V_{in}(t) - e_m(t) = Ri(t) + L\frac{d}{dt}i(t) \tag{15}$$

$$J_m\frac{d}{dt}\omega(t) = T(t) - T_L(t) \tag{16}$$

where $T(t)$ is the torque generated by the armature, k_t is the motor torque constant, $\omega_m(t)$ is the armature angular velocity, $e_m(t)$ is the back electro-magnetic force generated by the armature spinning at an angular velocity $\omega_m(t)$, $V_{in}(t)$ is the supply voltage, $i(t)$ is the current in the armature wire, and $T_L(t)$ is the load torque. For an unmanned motorcycle, unless a steering torque disturbance is introduced, $T_L(t) = M_\psi(t)$.

Combining Equations (6), (7) and (13)-(16) yields the block diagram between V_{in} and $\dot{\chi}$ shown in Figure 3. In this diagram, K is the stiffness coefficient of the shaft and θ_m is the armature angle. Neglecting the shaft torsion, ($K \to \infty$) yields:

$$\frac{\dot{\chi}(s)}{V_{in}(s)} = -\left[\frac{(k_t / R) \cdot N \cdot s \cdot p_2(s)}{(\tau_e s + 1)\left(J_m N^2 s^2 p_1(s) + p_5(s)\right) + (k_t k_b / R) N^2 \cdot s \cdot p_1(s)} \right] \qquad (17)$$

where $\tau_e = \frac{L}{R}$.

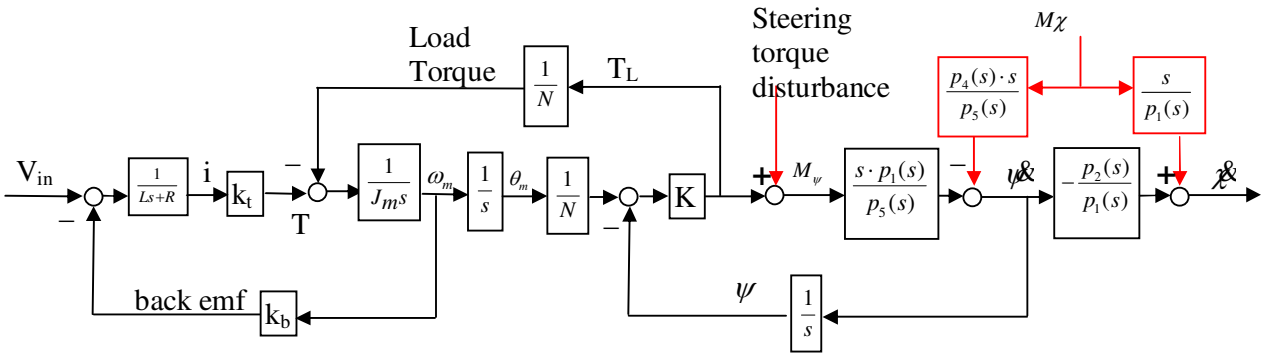

Figure 3: Block diagram depicting the relationship between the voltage applied to the steering motor V_{in} and the rate of change of the roll angle $\dot{\chi}$.

3. Controller design

Since both the roll angle and roll rate were measured, a cascaded control configuration was adopted, closing an inner loop on the roll rate and an outer loop on the roll angle (Figure 4). This configuration proved superior to a single compensator

based on the roll angle sensor only (not shown), due to fact that without using a dedicated sensor to measure the roll rate, the roll angle signal had to be differentiated numerically in the "derivative" component of the controller. Clearly, since the roll rate could be easily measured, this direct measurement was preferable over the numerical derivation of the roll angle signal that was sampled at only 50Hz. Note that the cascaded configuration was not strictly necessary (only the inner plant contains uncertainty and therefore a cascaded design can not divide the uncertainty burden between the two loops) and was chosen merely due to convenience considerations. Similar results could be obtained with a single feedback loop configuration incorporating both sensors.

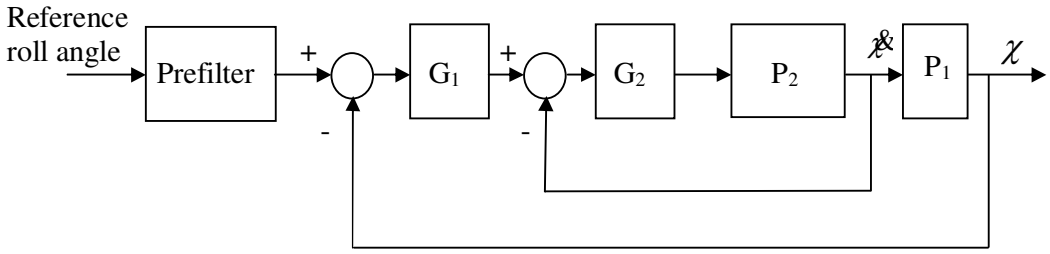

Figure 4: Cascaded control scheme. P_1 is a pure integrator and P_2 is the (uncertain) transfer function defined in Equation (17).

The objective of the control system was to stabilize the motorcycle for velocities ranging from 2.5 [m/s] to 6.5 [m/s] for the set of plants defined by the parameter uncertainties listed in Table 1. The servo specifications (desired response to reference roll angle step input) were chosen to correspond to the personal experience of the first author of this paper, who is a skilled and experienced motorcycle rider:

- Rise Time $\in$ [0.3 , 0.5] seconds

- Overshoot ≤ 20%
- Settling Time ≤ 5 seconds

Following the standard QFT procedure as implemented in the design software Qsyn (Gutman, 1996), these specifications were translated into the frequency domain assuming that the resulting closed-loop will behave approximately as a third-order system (Figure 5). In addition, the following sensitivity specification was imposed

$$|S| = \left| \frac{1}{\left(1 + G_1 \frac{G_2 P_2}{1 + G_2 P_2} P_1\right)} \right| \leq 8dB$$

which implies a minimum gain margin of ~4dB and phase margin of ~25 degrees for all plant cases.

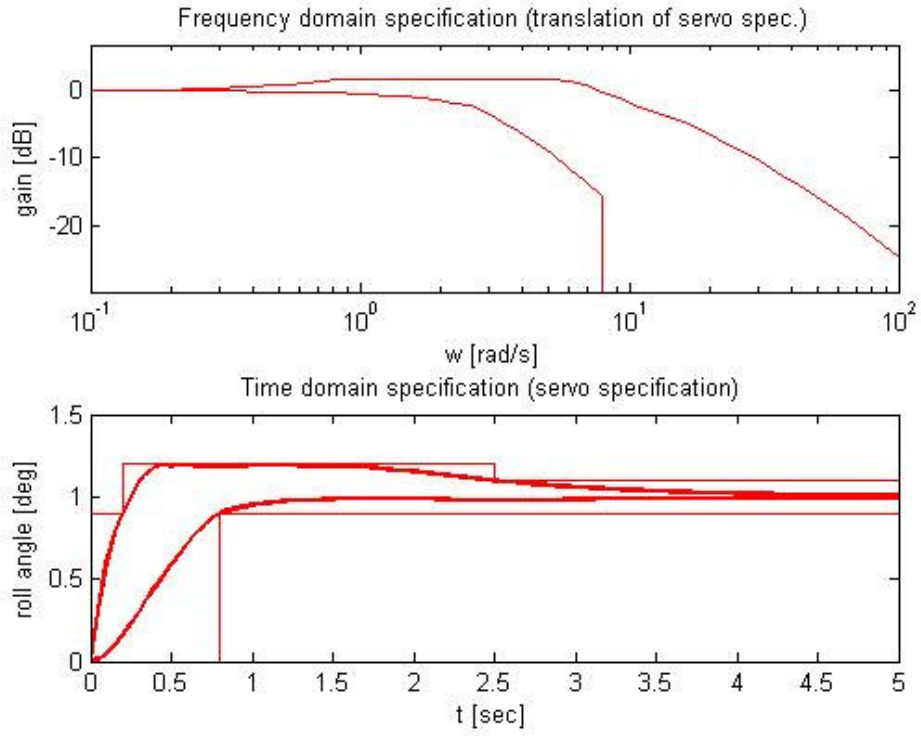

Figure 5: Servo specifications for the desired roll angle step response envelope in the time domain (lower frame), and translated to the frequency domain (upper frame), giving the desired gain envelope for the closed loop transfer function from roll reference angle to roll angle.

Before considering the control design itself, some important remarks must be made. Firstly, due to the relatively low resolution of the sensors (0.43º) and the relatively high level of low frequency noise, it was imperative to average the readings. The high sampling rate (10 kHz) could be achieved only if the control algorithm required as little computation time as possible. In other words, the micro-controller had to be operated in fixed-point mode, which in turn required that the controller be as simple (i.e. of low order) as possible. Secondly, there was significant noise only at frequencies much lower than the Nyquist frequency (5 kHz), which made it possible to sample the signals directly without pre-sampling filters. Finally, it must also be

noted that since the parameters of the motorcycle are speed-dependant, if a measurement of the velocity had been available, a gain-scheduling approach such as the one used by Sharp et al. (2004) could have been implemented. Such a measurement was not available in the present study due to budget limitations and the results presented below show that in the range of speeds investigated, the motorcycle can indeed be controlled using a fixed-parameter robust controller.

3.1 Design of the outer loop

Following the standard QFT procedure for cascaded feedback control (Horowitz and Sidi, 1973), the controller of the outer loop (G_1) was designed with the temporary assumption that the inner loop would be sufficiently regulated so that it could be approximated temporarily as 1. A simple proportional gain, namely G_1=15, was sufficient to bring the bandwidth within the desired range (Figure 6).

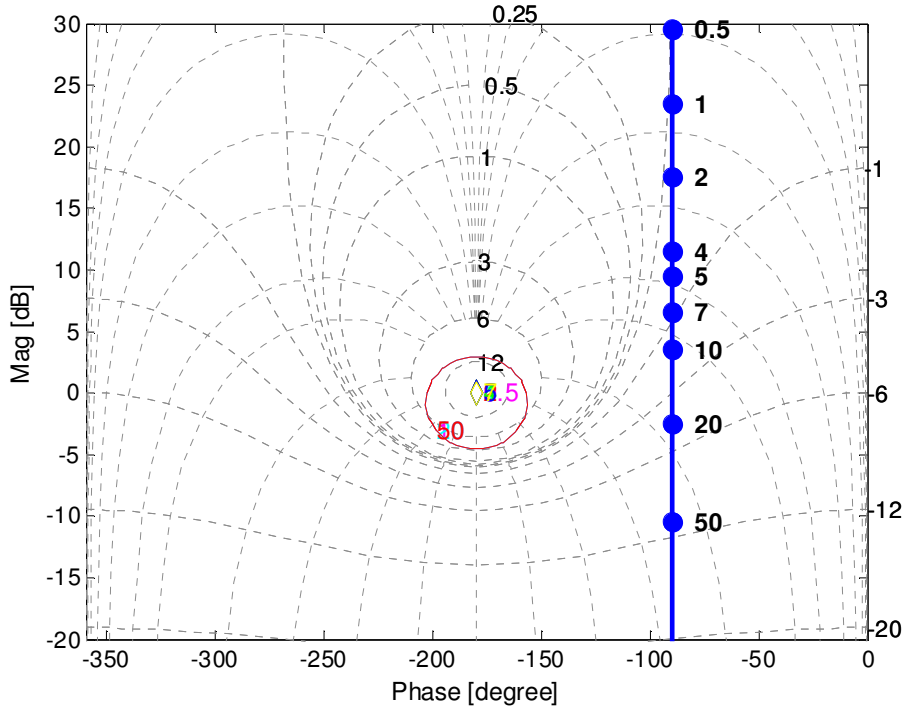

Figure 6: Nichols chart [dB vs. rad] showing the compensated nominal outer open loop (parameter values listed in Table 1) and sensitivity bounds (inner closed loop approximated as 1 at this stage).

3.2 Design of the inner loop and verification of the outer loop

After designing G_1 and computing the tolerance and sensitivity Horowitz-Sidi bounds for the inner loop (Figure 7), the inner controller G_2 was designed, yielding:

$$G_2(s) = 35\frac{\left(1+\frac{s}{3}\right)}{\left(1+\frac{s}{20}\right)} \tag{18}$$

Figure 7 shows that the inner loop with this controller meets the specifications.

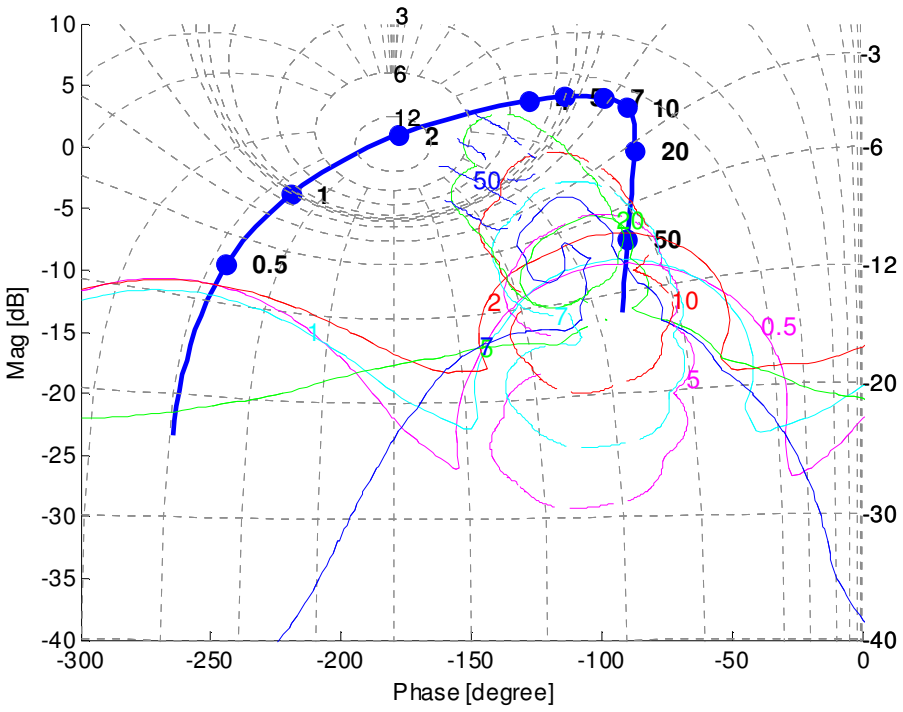

Figure 7: Nichols chart [dB vs. rad] showing the frequency function of the inner open loop including the nominal plant and the controller described in Equation (18) with the closed outer loop controlled by G_1=15 taken into account, together with Horowitz-Sidi bounds. The continuous thin lines correspond to the servo bounds and the dashed lines to the sensitivity bounds.

Figure 8 shows the actual recalculated outer loop with the controller G_2. It can be seen that although the actual inner loop differs significantly from unity (as assumed at the first design stage, Figure 6), the outer loop remains stable and meets the specifications. The reason is that in Section 3.1 the outer loop controller G_1 satisfies the specifications with a large margin, and as a consequence the ensuing inner loop specifications also become easy to satisfy with a large margin (Horowitz, 1993).

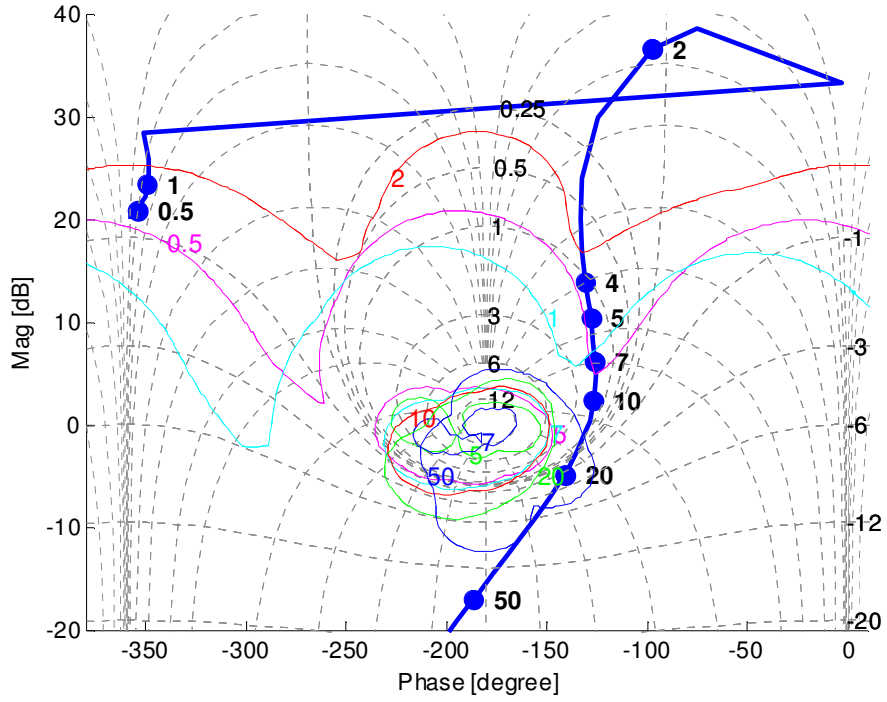

Figure 8: Nichols chart [dB vs. rad] showing the compensated outer loop (nominal), with closed inner loop, and bounds.

Finally, the following prefilter was added to adjust the system bandwidth according to the specifications (Figure 9):

$$F(s) = 1.1 \frac{1}{\left(1 + \frac{s}{5}\right)^2} \tag{19}$$

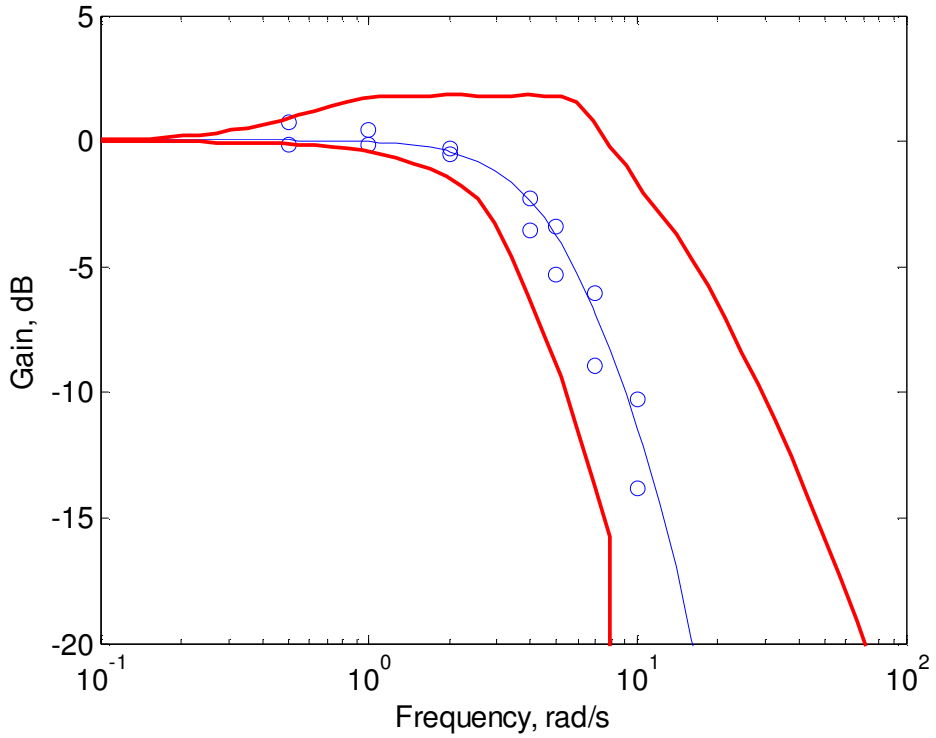

Figure 9: Gain of compensated closed loop with prefilter. The bold lines denote the range in which the closed loop must be in order to meet the design specifications. The solid line represents the nominal plant case. The circles show the range of the closed loop gain, for the frequencies at which the templates were computed.

Since the actual controllers were implemented on a digital microcontroller with a hold frequency of 50 Hz, G_2 and F were translated into their respective discrete-time forms using the matched zero-pole translation:

$$G_2(z) = 198.1\frac{(z\text{-}0.94194)}{(z - 0.67030)} \tag{20}$$

$$F(z) = \frac{0.009962}{(z^2\text{-}1.81\ z + 0.8187)} \tag{21}$$

Rechecking the loop-shaping design with these discrete controllers showed that the loops were stable and met the design requirements (not shown).

It must be emphasized that although much faster controllers with higher bandwidths could be synthesized to yield better simulated performances, in practice it was observed that such controllers resulted in awakening un-modeled vibration modes of the motorcycle due for instance to chassis flexibility and resonances due to nonlinearities in the loop such as the backlash of the steering motor gear. In addition, the controllers were intentionally kept as simple as possible since this allowed operation of the microcontroller in fixed-point mode, which ensured fast calculations. Attempts to implement more complex controllers that required longer calculations performed in floating-point mode showed that the disadvantage of the slower computations outweighed the theoretical benefits of such controllers.

4. Results

4.1 Simulation results

Figures 10 and 11 show the results of simulations based on Equations (3)-(17) after including in the Simulink model quantizers to account for the resolutions of the sensors and actuators. These Figures show the closed loop response to:

- a 10 degrees roll step command at time 0

- a 10 Nm steering torque disturbance between t = 1.5 and t=1.6 seconds. Such a disturbance may occur for instance when the front wheel hits an obstacle such as a stone that suddenly turns the steering assembly.

- a 50 Nm roll torque disturbance between t = 3.0 and t = 3.1 seconds. Such disturbance corresponds to someone shoving the motorcycle sideways, trying to trip it down, or to a sudden side-wind gust.

Figure 10 shows the steering angle obtained for random (constant) velocities and parameter values. In all cases, the settling time is well within the desired range and the motorcycle remains stable despite the strong disturbances. It can also be noted that the steady state roll angle does not necessarily coincide with the reference (10 degrees), which is not surprising since the outer controller does not include an integrator. Such an integrator would be detrimental since in practice the user that operates the motorcycle with the remote control closes an additional loop that includes an integrator, and the role of the present controller is solely to stabilize the system and regulate its transient behavior.

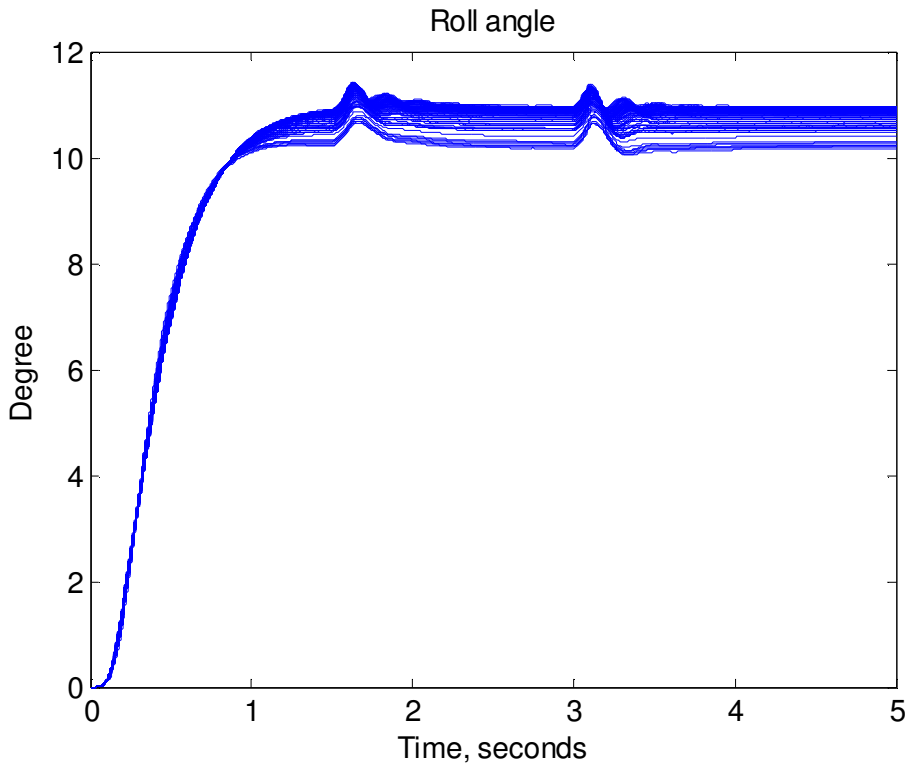

Figure 10: Results of 100 simulations with random values of the uncertain parameters and velocity. Disturbances: 10 [Nm] steering torque at t=1.5second, and 50 [Nm] roll torque at t=3 seconds. Each disturbance lasted 0.1 second.

Figure 11 shows in more detail the results obtained with nominal values of the parameters and forward velocities of 3 [m/s] and 5 [m/s]. It can be seen that the initial direction of steering is opposite to its steady state value (Top right frame), which is due to the non-minimum phase nature of the transfer function from the roll angle reference to the steering angle, known by motorcyclists as "counter steering". Also, it can be seen that the steering angle that corresponds to a given roll angle depends on the velocity. The bottom frame of Figure 11 shows that the voltage applied to the steering motor saturates only for a very short period of time immediately after the second disturbance, but the system remains stable.

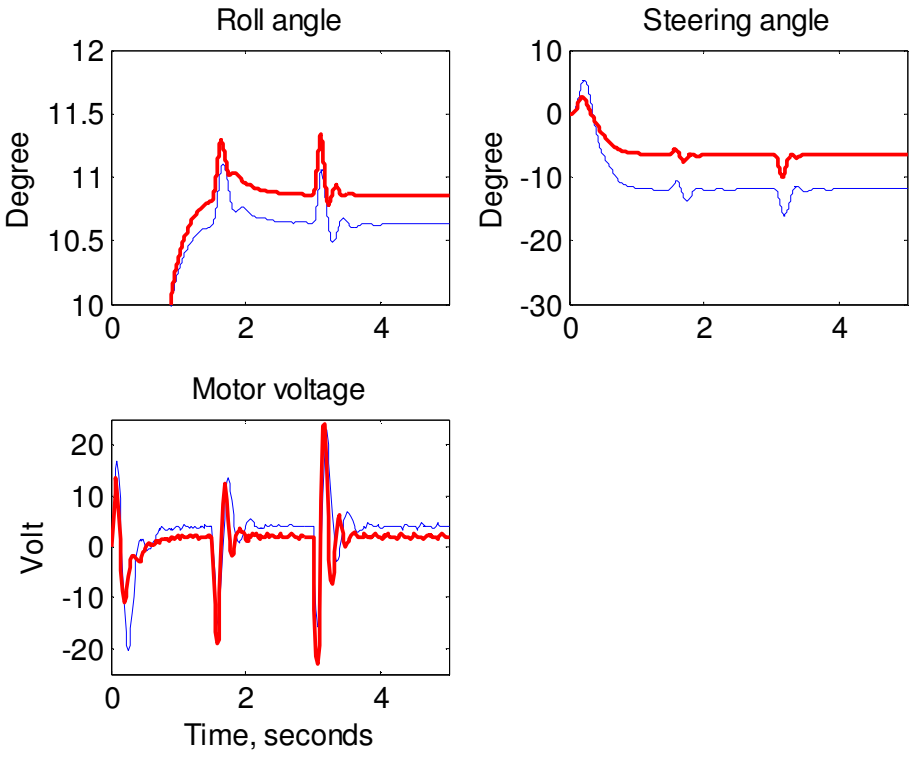

Figure 11: Simulation results for nominal parameter values and velocities of 3 [m/s] (thin) and 5 [m/s] (bold).

4.2 Experimental results

The prototype was tested on flat asphalt surface and the results can be best appreciated by viewing the video clips supplied in Annex "Electronic Annex 1 in the online version of this article". Some of these tests included shoving the motorcycle sideways while it was traveling at very low speed, or jumping over a 10cm-high ramp. During all these tests the motorcycle remained stable.

Due to the lack of memory of the on-board micro-controller sensor readings and actuator commands could not be stored for post-experimental analysis. However,

during some of the tests an additional data-logger was installed on the motorcycle, which enabled recording the roll angle at 100 [Hz] sampling rate. Some of this data is presented in Figures 12-14. Figure 12 shows the roll angle recorded during a run with the control joystick in neutral position. It can be seen that the controller stabilizes the motorcycle close to the vertical position. Small fluctuations, in the range of ±2° about zero roll angle, are most probably due to the fact that the motorcycle sensors read the vibration of the motorcycle caused by its engine, and these noisy readings entered the control loop. Figures 13 and 14 show responses to step changes in the roll angle command. Simulated step responses (based on Equations (3)-(17)) assuming a velocity of 4.5 [m/s] and the nominal parameter values as listed in Table 1 are also shown for comparison. The good agreement between the simulated and actual results is evident. Surprisingly, the real motorcycle responds slightly faster than predicted by the model. Of course, the simulation is based on a single plant out of the many plant cases existing due to the uncertainty in the parameters. However, running multiple simulations with various parameter combinations showed that none of these could yield a rise-time of approximately 0.3 [s], so that the reason for this faster response remains to be determined (it may result from unmodelled nonlinear properties of the tires). The slight difference in steady state gain is probably due to choosing one of the many plant cases for performing the simulation, as well as to the fact that the actual forward velocity of the motorcycle was not measured and could only be roughly estimated. Despite all these, there is a high degree of agreement between the simulations and the experimental results, which suggests that the model described in Section 2 captures successfully the dominant dynamics of the real motorcycle.

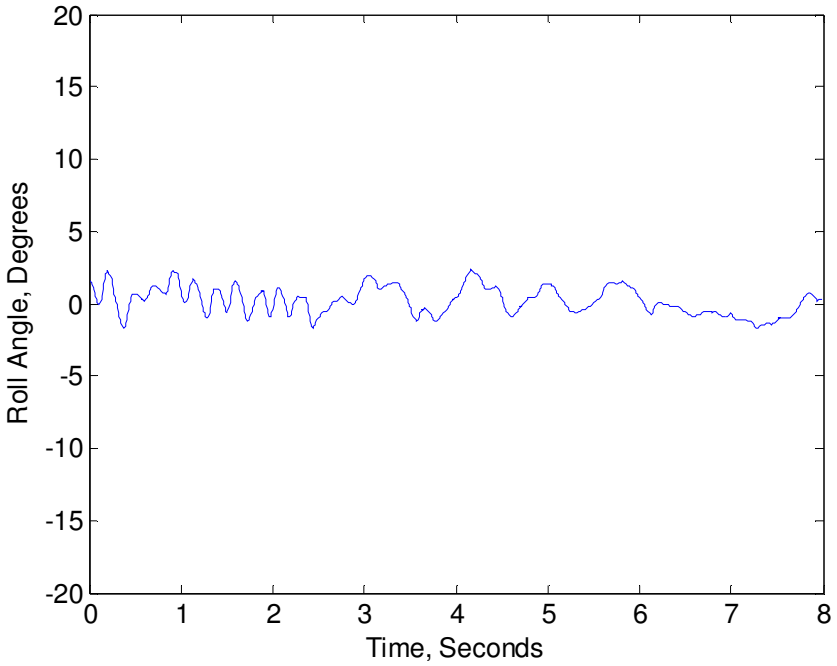

Figure 12: Experimental results. Signal from the roll angle sensor while the roll angle command was kept constant.

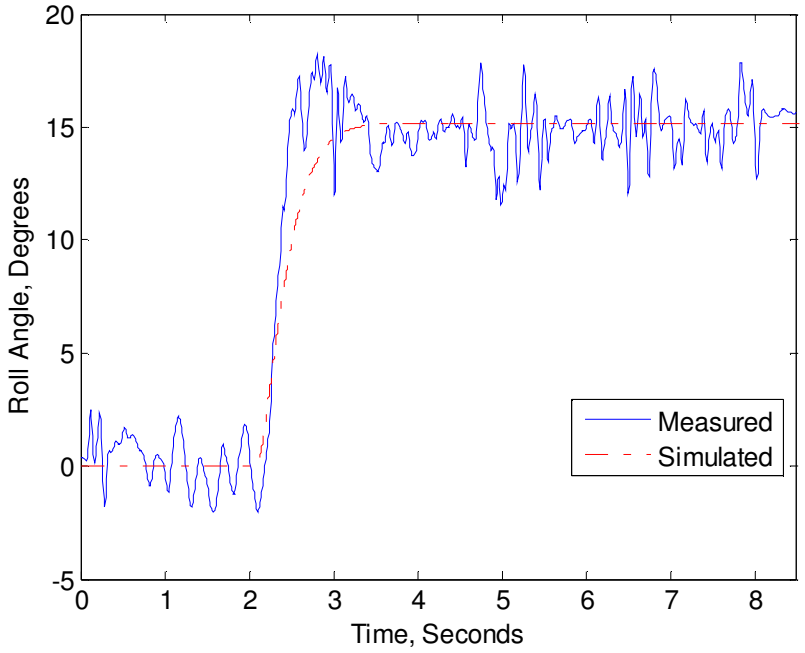

Figure 13: Measured (solid line) and simulated (dashed) roll angle in response to positive a step of the roll angle command

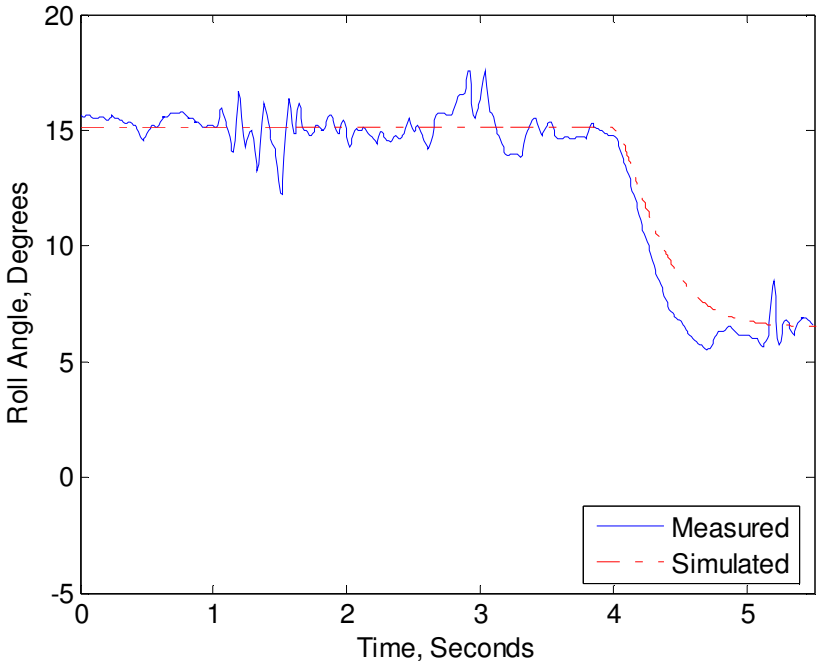

Figure 14: Measured (solid line) and simulated (dashed) roll angle in response to a negative step of the roll angle command

5. Conclusions

A robust controller that stabilizes an unmanned motorcycle for velocities ranging from 2.5 to 6.5 [m/s] was developed and validated. The QFT loop-shaping method led to a simple, low order cascaded controller that met the specifications. This controller was implemented on an experimental prototype that was successfully tele-operated on an outdoor asphalt surface.

References

Beznos AV, Formal'sky AM, Gurfinkel EV, Jicharev DN, Lensky AV, Savitsky KV,Tchesalin LS. Control of autonomous motion of two-wheel bicycle with gyroscopic stabilisation. Proceedings of the 1998 IEEE International Conference on Robotics & Automation.

Chidzonga RF, Eitelberg E Controlling velocity and steering for bicycle stabilization. Proceedings of the First African Control Conference (2003). Available at www.nt.ntnu.no/users/skoge/prost/proceedings/afcon03/Papers/010.pdf

Getz NH, Marsden JE. Control for an autonomous bicycle. Proceedings of the 1995 IEEE International Conference on Robotics & Automation.

Gutman PO. Qsyn – *the* toolbox for robust control systems design for use with MATLAB–User'sGuide (1996). Available at http://www.math.kth.se/optsyst/forskning/forskarutbildning/5B5782/index.html

Gutman P-O. Robust and adaptive control - fidelity or a free relationship? Systems and Control Letters 2003, 49: 9-19.

Horowitz IM. Quantitative Feedback Design Theory, 1993.

Horowitz IM, Sidi M. Synthesis of feedback systems with large plant ignorance for prescribed time-domain tolerances. International Journal of Control 1972, 16: 287-309.

Iuchi K, Niki H, Murakami T. Attitude control of bicycle motion by steering angle and variable COG control. Proceedings of the 32nd IEEE/IECON Annual Conference (2005).

Meijaard JP, Papadopoulos JM, Ruina A, Schwab AL. Linearized dynamics equations for the balance and steer of a bicycle: a benchmark and review. Proceedings of the Royal Society A. 2007; 463: 1955-1982.

Miyagishi S, Kageyama I, Takama K, Baba M and Uchiyama H. Study on construction of a rider robot for two-wheeled vehicle. JSAE Review 2003; 24: 321-326.

Nenner U. Control of an unmanned motorcycle robot. M.Sc Thesis. Technion – Israel Institute of Technology (2009).

Nenner U, Linker R, Gutman PO. Robust stabilization of an unmanned motorcycle. Proceedings of the IEEE CIS-RAM Conference. Chengdu, China (2009).

Ruijs PAJ and Pacejka HB. Recent research in lateral dynamics of motorcycles. Vehicle System Dynamics 1985; 15: 467-480.

Schwab AL, Meijaard JP and Papadopoulos JM. Benchmark Results on the linearized equations of motion of an uncontrolled bicycle. Proceedings of the Second Asian Conference on Multibody Dynamics 2004.

Sharp, RS, The stability and control of motorcycles, Journal of Mechanical Engineering Science 1971, 13: 316-329.

Sharp RS. Stability, control and steering response of motorcycles. Vehicle System Dynamics 2001, 35: 291-318.

Sharp RS. Optimal linear time-invariant preview steering control for motorcycles. Vehicle System Dynamics 2006; 44: 329-340.

Sharp RS. Motorcycle steering control by road preview. Journal of Dynamic Systems, Measurements, and Control 2007a; 129: 373-381.

Sharp RS. Optimal preview speed-tracking control for motorcycles. Multibody systems dynamics 2007b; 18: 397-411.

Sharp RS, Evangelou S, Limebeer DJN. Advances in the modeling of motorcycle dynamics. Multibody systems dynamics 2004; 12: 251-283.

Sharp RS, Limebeer DJN. A motorcycle model for stability and control analysis. Multibody systems dynamics 2001; 6: 123-142.

Tanaka Y, Murakami T. Self sustaining bicycle robot with steering controller. Proceedings of the 8th IEEE International workshop on Advanced Motion Control (2004).

Weir DH. Motorcycle handling dynamics and rider control and the effect of design configurations on response and performance. PhD Thesis, University of California, LA, 1972.

Yi J, Song D, Levandowski A and Jayasuriya S. Trajectory tracking and balance stabilization control of autonomous motorcycles. Proceedings of the 2006 IEEE International Conference on Robotics & Automation.

Figure captions

Figure 1: Side view of the experimental prototype

Figure 2: Motorcycle physical parameters.

Figure 3: Block diagram depicting the relationship between the voltage applied to the steering motor V_{in} and the rate of change of the roll angle $\dot{\phi}$.

Figure 4: Cascaded control scheme. P_1 is a pure integrator and P_2 is the (uncertain) transfer function defined in Equation (17).

Figure 5: Servo specifications for the desired roll angle step response envelope in the time domain (lower frame), and translated to the frequency domain (upper frame), giving the desired gain envelope for the closed loop transfer function from roll reference angle to roll angle.

Figure 6: Nichols chart [dB vs. rad] showing the compensated nominal outer open loop (parameter values listed in Table 1) and sensitivity bounds (inner closed loop approximated as 1 at this stage).

Figure 7: Nichols chart [dB vs. rad] showing the frequency function of the inner open loop including the nominal plant and the controller described in Equation (18) with the closed outer loop controlled by G_1=15 taken into account, together with Horowitz-Sidi bounds. The continuous thin lines correspond to the servo bounds and the dashed lines to the sensitivity bounds.

Figure 8: Nichols chart [dB vs. rad] showing the compensated outer loop (nominal), with closed inner loop, and bounds.

Figure 9: Gain of compensated closed loop with prefilter. The bold lines denote the range in which the closed loop must be in order to meet the design specifications. The

solid line represents the nominal plant case. The circles show the range of the closed loop gain, for the frequencies at which the templates were computed.

Figure 10: Results of 100 simulations with random values of the uncertain parameters and velocity. Disturbances: 10 [Nm] steering torque at t=1.5second, and 50 [Nm] roll torque at t=3 seconds. Each disturbance lasted 0.1 second.

Figure 11: Simulation results for nominal parameter values and velocities of 3 [m/s] (thin) and 5 [m/s] (bold).

Figure 12: Experimental results. Signal from the roll angle sensor while the roll angle command was kept constant.

Figure 13: Measured (solid line) and simulated (dashed) roll angle in response to positive a step of the roll angle command.

Figure 14: Measured (solid line) and simulated (dashed) roll angle in response to a negative step of the roll angle command.